

MODELING AND ANALYSIS OF CANTILEVERED PIEZOELECTRIC ENERGY HARVESTERS

Carlos De Marqui Junior, demarqui@sc.usp.br

Department of Aeronautical Eng., Engineering School of Sao Carlos, University of Sao Paulo, SP, Brazil

Alper Erturk, erturk@vt.edu

Center for Intelligent Material Systems and Structures, Department of Eng. Science and Mechanics, Virginia Tech, VA, USA

Daniel J. Inman, dinman@vt.edu

Center for Intelligent Material Systems and Structures, Department of Mechanical Eng., Virginia Tech, VA, USA

Abstract. *The electromechanically coupled finite element (FE) modeling of a cantilevered plate-like wing with embedded piezoceramics is presented for energy harvesting. The goal in this research field is to power small electronic components by converting waste vibration energy available in their environment into electrical energy. Cantilevered beams and plates with piezoceramic layers are commonly employed as piezoelectric energy harvesters. Generalized Hamilton's principle for electroelastic bodies is reviewed and the FE model is derived based on the Kirchhoff plate assumptions as typical piezoelectric energy harvesters are thin structures. The presence of conductive electrodes is taken into account in the FE model. The FE model is also combined with a unsteady vortex lattice aerodynamic model resulting in a piezo-aero-elastic model. Three case studies are presented here. First the electromechanical predictions of the FE model are verified against the analytical solution for a unimorph cantilever and then against the experimental and analytical results of a bimorph cantilever plate with a tip mass reported in the literature. In the third case study piezo-aero-elastic simulations are performed to investigate the electrical and mechanical output of a generator wing for several airflow speeds. In addition to piezoelectric power generation, the effect of resistive shunt damping on the aeroelastic response of the generator wing is observed.*

Keywords: *energy harvesting, piezoelectric, piezo-aero-elasticity*

1. INTRODUCTION

Multifunctional structures are one of the emerging areas of research that can lead to more efficient Micro Air Vehicles (MAVs) and Unmanned Air Vehicles (UAVs) (Pines and Bohorquez, 2006). Multifunctional structures perform additional tasks besides their primary function (Dodemant, 2006). Based on the concept of vibration-based energy harvesting an additional functionality can be integrated into the wing structure of an UAV or MAV: provide an additional source of electrical energy for these aircraft by converting vibrations available in their environment to electricity (Sodano et al., 2004; Beeby et al., 2006; Priya, 2007; Anton and Sodano, 2007; Cook-Chennault et al., 2008). Generating usable electrical energy to run small electronic devices such as sensor systems during a flight has the practical value of relieving auxiliary power drains for these aircraft. A possible source of energy for UAVs and MAVs is the mechanical vibration energy due to unsteady aerodynamic loads during the flight (Anton and Inman, 2008) and due to ground excitation in perching (Magoteaux et al., 2008, Erturk et al., 2008a). Piezoelectric transduction has received the most attention for vibration-based energy harvesting resulting in four review articles appearing in the last four years (Sodano et al., 2004; Priya, 2007; Anton and Sodano, 2007; Cook-Chennault et al., 2008).

In practice, cantilevered beams and plates with piezoceramic layers are employed as piezoelectric energy harvesters. Researchers have proposed various models to represent the electromechanical behavior of piezoelectric energy harvesters, which range from lumped parameter models (Roundy et al., 2003; du Toit et al., 2005) to Rayleigh-Ritz type approximate distributed parameter models (Sodano et al., 2004; du Toit et al., 2005) as well as analytical distributed parameter solution attempts (Chen et al., 2006; Lin et al., 2007). More recently, the analytical distributed parameter solutions for unimorph (Erturk and Inman, 2008b) and bimorph beam-type (Erturk and Inman, 2009) piezoelectric harvester configurations with closed-form expressions have been presented. However, aspect ratios of piezoelectric harvesters in several cases are plate-like and predicting the power output to general (symmetric and asymmetric) excitations requires a plate-type formulation. An electromechanically coupled finite element (FE) plate model for predicting the mechanical response and electrical output (voltage, current and power) of piezoelectric energy harvester plates is presented in De Marqui et al. (2009). The generalized Hamilton's principle for electroelastic bodies is reviewed and the FE model is derived based on the Kirchhoff plate assumptions as typical piezoelectric energy harvesters are thin structures. Presence of conductive electrodes is taken into account in the FE model. A resistive electrical load is considered in the electrical domain.

Three case studies are presented in this paper using the electromechanically coupled FE model. First the FE model is verified against the analytical solution for a unimorph cantilever (one piezoceramic layer perfectly bonded to a substructure layer) under base excitation found in the literature. Electromechanical frequency response functions

(voltage, current, power and relative tip motion FRFs) obtained using the FE model are compared with the analytically obtained FRFs. As a second case study, the analytical and experimental FRFs of a bimorph cantilever (a brass substructure bracketed by two piezoceramic layers and electrodes connected in series to the external electrical load) with a tip mass are predicted by using the FE model. As a third case study, the piezo-aero-elastic modeling of a cantilevered plate-like wing with embedded piezoceramics is briefly presented for energy harvesting. The electrical and mechanical outputs are obtained for several airflow speeds. In addition to piezoelectric power generation, the effect of resistive shunt damping on the aeroelastic response of the generator wing is observed.

2. ELECTROMECHANICALLY COUPLED FINITE ELEMENT MODEL

Using the linear-elastic constitutive relation for an isotropic substructure material and the linear electroelastic constitutive relation for a transversely isotropic piezoceramic material (used here in the plane-stress form, De Marqui et al. (2009)) the generalized Hamilton's principle for a piezoelectric energy harvester becomes,

$$\int_{t_1}^{t_2} \left[\int_{V_s} \rho_s \delta \dot{\mathbf{u}}^t \dot{\mathbf{u}} dV_s + \int_{V_p} \rho_p \delta \dot{\mathbf{u}}^t \dot{\mathbf{u}} dV_p - \int_{V_s} \delta \mathbf{S}^t \mathbf{c}_s \mathbf{S} dV_s - \int_{V_p} \delta \mathbf{S}^t \mathbf{c}_p^E \mathbf{S} dV_p + \int_{V_p} \delta \mathbf{S}^t \mathbf{e}^t \mathbf{E} dV_p + \int_{V_p} \delta \mathbf{E}^t \mathbf{e} \mathbf{S} dV_p + \int_{V_p} \delta \mathbf{E}^t \boldsymbol{\epsilon}^S \mathbf{E} dV_p + \sum_{i=1}^{nf} \delta \mathbf{u}(x_i, y_i, t) \cdot \mathbf{f}(x_i, y_i, t) + \sum_{j=1}^{nq} \delta \varphi(x_j, y_j, t) q(x_j, y_j, t) \right] dt = 0 \quad (1)$$

where \mathbf{u} is the vector of mechanical displacements, \mathbf{c}_s is the 2-D elastic stiffness matrix obtained as function of the Poisson's ratio ν_s and the Young's modulus Y_s of the substructure material, \mathbf{S} is the vector of mechanical strain components, \mathbf{T} is the vector of mechanical stress components, \mathbf{D} is the vector of electric displacement components, \mathbf{E} is the vector of electric field components, \mathbf{c}_p is the 2-D elastic stiffness matrix obtained in terms of the 3-D components, \mathbf{e} is the matrix of piezoelectric constants, $\boldsymbol{\epsilon}$ is the matrix of permittivity components, superscript E and S denote that the parameters are measured at constant electric field and constant strain, respectively, ρ is the mass density, V is the volume, t denotes transpose when it is used as a superscript (otherwise it stands for the time) and an over-dot represents differentiation with respect to time. Here and hereafter, subscripts s and p stand for the substructure and piezoceramic layers, respectively; \mathbf{f} is the set of discrete mechanical forces applied at locations (x_i, y_i) , q the set of discrete electric charge outputs *extracted* at locations (x_j, y_j) , nf is the number of discrete mechanical forces, φ_j is the scalar electrical potential and nq is the number of discrete electrode pairs.

Typical piezoelectric energy harvesters, as depicted in Fig. 1, are designed to have cantilevered boundary conditions. The substructure and the piezoceramic layer of the unimorph piezoelectric energy harvester are assumed to be perfectly bonded to each other. The piezoceramic layer is bracketed by continuous and perfectly conductive electrodes with negligible thickness. A resistive load is considered in the electrical domain and the purpose is to estimate the electrical power converted from the mechanical vibrations of the energy harvester plate. The electromechanically coupled FE model can be easily modified to represent a bimorph harvester as stated in the end of this section.

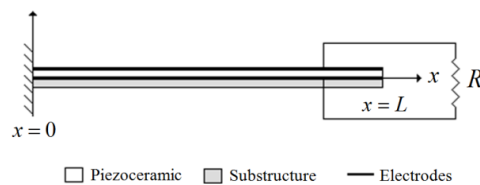


Figure 1. A unimorph piezoelectric harvester with clamped-free boundary conditions.

A rectangular finite element with four nodes and three mechanical degrees of freedom per node (namely the displacements u_x , u_y and u_z in x , y and z directions) is used to model the substructure and the piezoceramic layer. Based on the assumption that each finite element of the piezoceramic layer is completely covered with perfectly conductive electrodes, one electrical degree of freedom (voltage v_p across the electrodes) is added to the element for modeling the electrical domain of these elements.

Based on the Kirchhoff plate theory, shear deformations and rotary inertias of the finite elements are neglected and in-plane displacements (u_x and u_y) are assumed to be due to the bending (cross-section rotation) of the plate only. The displacement field is then

$$\mathbf{u} = \begin{Bmatrix} u_x \\ u_y \\ u_z \end{Bmatrix} = \left\{ -z \frac{\partial w}{\partial x} \quad -z \frac{\partial w}{\partial y} \quad w \right\}^t \quad (2)$$

where the displacement components u_x , u_y and u_z at a thickness level z from the reference (neutral) surface are given in terms of the transverse deflection (w) of the reference surface.

The mechanical strain components can be written as

$$\mathbf{S} = \begin{Bmatrix} S_x \\ S_y \\ 2S_{xy} \end{Bmatrix} = \left\{ \frac{\partial u_x}{\partial x} \quad \frac{\partial u_y}{\partial y} \quad \frac{\partial u_x}{\partial y} + \frac{\partial u_y}{\partial x} \right\}^t = -z \left\{ \frac{\partial^2 w}{\partial x^2} \quad \frac{\partial^2 w}{\partial y^2} \quad 2 \frac{\partial^2 w}{\partial x \partial y} \right\}^t \quad (3)$$

The vector of nodal variables for the rectangular finite element can be defined as

$$\boldsymbol{\Psi} = \{w_1 \quad \theta_{x1} \quad \theta_{y1} \quad w_2 \quad \theta_{x2} \quad \theta_{y2} \quad w_3 \quad \theta_{x3} \quad \theta_{y3} \quad w_4 \quad \theta_{x4} \quad \theta_{y4}\}^t \quad (4)$$

where w_k is the transverse displacement for of node k , $\theta_{xk} = \partial w / \partial x|_{x_k, y_k}$ and $\theta_{yk} = -\partial w / \partial x|_{x_k, y_k}$ are the bending rotations. To derive the element matrices, the displacement field \mathbf{u} described by Eq. (2) and consequently the strain components \mathbf{S} described by Eq. (3) have to be expressed as functions of nodal variables. This is done expressing the transverse displacement (consequently the cross-section rotations) and the vector of curvatures in terms as,

$$\left\{ \frac{\partial w}{\partial x} \quad \frac{\partial w}{\partial y} \quad w \right\}^t = \mathbf{B}_\eta \boldsymbol{\Psi} \quad (5)$$

$$\left\{ \frac{\partial^2 w}{\partial x^2} \quad \frac{\partial^2 w}{\partial y^2} \quad 2 \frac{\partial^2 w}{\partial x \partial y} \right\}^t = \mathbf{B}_\kappa \boldsymbol{\Psi} \quad (6)$$

where are \mathbf{B}_η and \mathbf{B}_κ are 3×12 matrices defined as interpolation functions.

The piezoceramics are assumed poled in the thickness direction (z -direction). Therefore the vector of electric field components can be expressed as,

$$\mathbf{E} = -\mathbf{B}_E v_p \quad (7)$$

$$\text{where } \mathbf{B}_E = \left\{ 0 \quad 0 \quad \frac{1}{h_p} \right\}^t.$$

The foregoing electrical relation and the previous mechanical equations (Eqs. 2 to 6) are used in the generalized Hamilton's principle given by Eq. (1) to give the element mass (\mathbf{m}) and stiffness (\mathbf{k}) matrices (12×12), electromechanical coupling ($\boldsymbol{\theta}$) and external force (\mathbf{f}) vectors (12×1) and the scalar capacitance term (c_p). The global equations of motion are then obtained by assembling the element matrices resulting in the equations,

$$\mathbf{M}\ddot{\boldsymbol{\Psi}} + \mathbf{C}\dot{\boldsymbol{\Psi}} + \mathbf{K}\boldsymbol{\Psi} - \tilde{\boldsymbol{\Theta}}v_p = \mathbf{F} \quad (8a)$$

$$C_p \dot{v}_p + \frac{v_p}{R_l} + \tilde{\boldsymbol{\Theta}}^t \dot{\boldsymbol{\Psi}} = 0 \quad (8b)$$

where \mathbf{M} is the global mass matrix ($n_m \times n_m$), \mathbf{K} is the global stiffness matrix ($n_m \times n_m$) and $\tilde{\boldsymbol{\Theta}}$ is the global electromechanical coupling vector ($n_m \times 1$), C_p is the global capacitance term (scalar), \mathbf{F} is the global vector of mechanical forces ($n_m \times 1$), $\boldsymbol{\Psi}$ is the global vector of mechanical coordinates ($n_m \times 1$), v_p is the voltage output measured from the electrodes and R_l is the external resistive load. Equations (8a) and (8b) are modified versions of the originally obtained equations. A transformation that accounts the presence of full electrodes bracketing the

piezoceramics was used to modify the original equations (De Marqui et al., 2009). Here, n_m is the number of mechanical degrees of freedom of the harvester plate. In Eq. (8a), the global mechanical damping matrix ($n_m \times n_m$) is assumed to be proportional to the mass and stiffness matrices:

$$\mathbf{C} = \alpha\mathbf{M} + \beta\mathbf{K} \quad (9)$$

where α and β are the constant of proportionality.

This FE model is easily modified to represent a bimorph harvester (one substructure layer bracketed by two identical piezoceramic layers). The mass, stiffness and damping matrices have to consider the additional piezoceramic layer. For the bimorph in series connection case treated here the piezoceramic layers are assumed poled in the opposite direction, the effective electromechanical coupling vector is equal to that of one piezoceramic layer and the effective capacitance is one half of the capacitance of one piezoceramic layer (Erturk and Inman, 2009).

3. UNSTEADY VORTEX-LATTICE AERODYNAMIC MODEL

The aerodynamic model used in this paper is accomplished with the unsteady vortex-lattice method (UVLM) (Benini et al., 2004). A planar vortex ring is associated with each rectangular panel of the body itself and its wake. The aerodynamic loads on the plate-like wing are obtained by combining the vortex singularities with the incompressible potential flow around the body. The leading segment of each planar vortex ring is placed at the quarter chord point of the panel. A control point is placed at the three-quarter chord of each panel. The boundary condition is verified at the control points and are given by the equation,

$$\left(\nabla\phi + \mathbf{v}_{motion} + \mathbf{v}_{wake} \right) \cdot \mathbf{n} = 0 \quad (10)$$

where $\Delta\phi$ is the gradient of the velocity potential corresponding to the perturbed velocity induced by the vortex singularities on the wing, \mathbf{v}_{motion} is the velocity due to wing motion, \mathbf{v}_{wake} is the velocity induced by the wake on the control points and \mathbf{n} represents the normal direction to the surface of wing at the control points. The boundary condition has to be satisfied at each time step of this unsteady solution and this way the correct values for the circulation of vortex singularities are obtained.

The term \mathbf{v}_{motion} is given by the free stream velocity plus velocities of the control points due to structural deformations of the wing. The velocity induced at an arbitrary point by a straight segment of a vortex ring is given by the Biot-Savart law. This way the perturbed velocity induced by the vortex singularities on the wing depends on the geometrical characteristics of the aerodynamic grid (position of vortex ring corners and control points) and on the circulation values (the unknowns at each time step of the numerical solution scheme). The free stream is always known; the velocities of the control points are determined by solving the electromechanically coupled FE model in time domain. The velocities induced by the wake \mathbf{v}_{wake} are obtained using Biot-Savart law. At each time step, new vortex rings are formed and shed from the trailing edge to the wake. The Kutta condition is satisfied imposing the circulation values of the most recently shed vortex rings at each time step as the same as those at the trailing edge (shedding vortices) in the previous time step. The circulation of the vortex rings on the wake remains unchanged and the wake carries no aerodynamic loads. The circulation values for the vortex rings placed on the wing are obtained from the solution of a linear system of equations obtained from Eq. (10). Therefore the pressure distribution is determined and the aerodynamic load for each panel can be calculated from the unsteady Bernoulli equation.

4. PIEZO-AERO-ELASTIC MODEL

The equations of motion obtained from the FE formulation can be represented in modal domain as

$$\bar{\mathbf{M}}\ddot{\boldsymbol{\eta}} + \bar{\mathbf{C}}\dot{\boldsymbol{\eta}} + \bar{\mathbf{K}}\boldsymbol{\eta} - \boldsymbol{\Phi}'\tilde{\boldsymbol{\Theta}}v_p = \boldsymbol{\Phi}'_a\mathbf{F}_a \quad (11a)$$

$$C_p\dot{v}_p + \frac{v_p}{R_l} + \tilde{\boldsymbol{\Theta}}'\boldsymbol{\Phi}'\dot{\boldsymbol{\eta}} = 0 \quad (11b)$$

where $\boldsymbol{\eta}$ is the vector of modal coordinates, $\boldsymbol{\Phi}$ is the modal matrix (mass normalized so that the modal mass $\bar{\mathbf{M}}$ is the identity matrix), $\bar{\mathbf{C}}$ is the diagonal modal damping matrix, $\bar{\mathbf{K}}$ is the diagonal modal stiffness matrix, \mathbf{F} is the vector of aerodynamic loads and $\boldsymbol{\Phi}'_a$ is the modal matrix in aerodynamic coordinates. Note that in this equation $\boldsymbol{\Phi}'_a$ accounts for the conversion of aerodynamic loads to the FE nodes.

In addition, structural displacements obtained at the nodes of FE mesh at each time step have to be obtained at the corners of vortex rings (aerodynamic mesh) for calculation of the aerodynamic loads. This way another transformation matrix is introduced to convert the modal coordinates to the corners of the vortex rings

$$\mathbf{x}_a = \mathbf{\Phi}_a^* \boldsymbol{\eta} \quad (12)$$

where \mathbf{x}_a is the vector of aerodynamic coordinates and the matrices $\mathbf{\Phi}_a$ and $\mathbf{\Phi}_a^*$ are interpolated in this work using surface splines.

The equations of motion (Eqs. 11a and 11b) can be written as a system of $2n + 1$ first order ordinary-differential equations, where n is the number of modes taken into account in the solution. The $2n + 1$ ordinary-differential equations are then solved using the Adams-Bashforth-Moulton predictor-corrector scheme that accounts for the interaction between aerodynamic and electromechanical domains (Lambert, 1991).

5. RESULTS

This section presents case studies using the electromechanical FE model and the piezo-aero-elastic model. In the first case study, the FE model is verified against the analytical results from the closed-form solution given by Erturk and Inman (2008b) for a unimorph harvester under base excitation. The second case study aims to predict the analytical and experimental results for a bimorph harvester with a tip mass presented by Erturk and Inman (2009). The third case study presents the piezo-aero-elastic behavior of a cantilevered plate-like wing with two identical layers of (PZT-5A) embedded into the top and on the bottom of the plate.

The material and electromechanical properties for PZT-5A (used in all cases) are given in Table 1. It is worthwhile mentioning that manufacturers typically provide limited number of properties for piezoelectric ceramics. For instance, in the predictions of their analytical model, Erturk and Inman (2008b) used the data provided by Piezo Systems Inc. as the data provided by the manufacturer was sufficient for a beam-type formulation. However, the plate-type formulation given here requires more than what is provided in the manufacturer's data sheet (see, for instance, the properties required for the calculation of the plane-stress elastic, piezoelectric and dielectric components in De Marqui et al. (2009)). Therefore, the 3-D properties of PZT-5A (www.efunda.com) displayed in Table 1 are used here.

Table 1. Material and electromechanical properties of PZT-5A

Mass density (kg/m ³)	7800	c_{33}^E (GPa)	110.9
Permittivity (nF/m)	$1800 \times \epsilon_0$	c_{66}^E (GPa)	22.7
c_{11}^E, c_{22}^E (GPa)	120.3	e_{31}, e_{32} (C/m ²)	-5.2
c_{12}^E (GPa)	75.2	e_{33} (C/m ²)	15.9
c_{13}^E, c_{23}^E (GPa)	75.1		

5.1. Case study 1 - Unimorph harvester under base excitation

The numerical input data of the unimorph studied by Erturk and Inman (2008b) is shown in Table 2. The results of the FE model are compared against the analytical solution in this section. The piezoceramic layer uniformly covers the substructure layer and the conductive electrodes are connected to a resistive electrical load as depicted in Fig. 1. Expressions for electromechanical FRFs, in this case the voltage across the resistive load and relative tip motion, are obtained from the equations of motion defined in the FE model (Eqs. 8a and 8b). The material, electromechanical and geometric properties given in Tables 1 and 2 are used in the coupled FE simulations.

Table 2. Geometric and material properties of the unimorph harvester

Length of the beam (m)	0.1	Mass density of the substructure (kg/m ³)	2750
Width of the beam (m)	0.02	Thickness of the PZT (m)	0.004
Thickness of the substructure (m)	0.005	Proportional constant – α (rad/s)	4.886
Young's modulus of the substructure (GPa)	70.0	Proportional constant – β (s/rad)	1.2433×10^{-5}

The excitation is due to the harmonic motion of the base in the transverse direction, $w_B(t) = Y_0 e^{j\omega t}$ (where $w_B(t)$ is the base displacement, Y_0 is its amplitude, ω is the excitation frequency and j is the unit imaginary number). At steady state, the voltage output – to – base acceleration FRF can be obtained from Eqs. (8a) and (8b) as

$$\frac{v_p(t)}{a_B(t)} = \frac{v_p(t)}{-\omega^2 Y_0 e^{j\omega t}} = j\omega \left(\frac{1}{R_l} + j\omega C_p \right)^{-1} \tilde{\Theta}^t \left(-\omega^2 \mathbf{M} + j\omega \mathbf{C} + \mathbf{K} + j\omega \left(\frac{1}{R_l} + j\omega C_p \right)^{-1} \tilde{\Theta} \tilde{\Theta}^t \right)^{-1} \mathbf{m}^* \quad (13)$$

where \mathbf{m}^* is an $(n_m \times 1)$ mass vector obtained from the global forcing term \mathbf{F} for the base excitation problem (De Marqui et al, 2009). As discussed in the literature (Erturk and Inman, 2008), if the base is vibrating in the transverse direction (z -direction), the effective force on the structure is due to the inertia of the structure in the same direction. Here, it is assumed that both layers (piezoceramic and substructure) have the same mesh and the nodes are coincident.

The electric current FRF is obtained by dividing the voltage FRF to the load resistance of the energy harvesting circuit. The electrical power FRF is the product of voltage and current FRFs and it is defined as the ratio of electrical power output to square of the base acceleration. Note that the modulus form of Eq. (13) is the peak voltage FRF (not the root mean square value). Therefore the electrical power obtained from this voltage FRF is the peak power and the average power amplitude is half of the peak power.

The relative tip motion FRF is defined as the ratio of the amplitude of the displacement at the tip of the beam (relative to the base) to the amplitude of base displacement input and its is obtained from Eqs. (8a) and (8b) as

$$\frac{\mathbf{w}_{rel}}{Y_0 e^{j\omega t}} = \omega^2 \left(-\omega^2 \mathbf{M} + j\omega \mathbf{C} + \mathbf{K} + j\omega \left(\frac{1}{R_l} + j\omega C_p \right)^{-1} \tilde{\Theta} \tilde{\Theta}^t \right)^{-1} \mathbf{m}^* \quad (14)$$

which defines a vector for the vibration response of all coordinates. Here, the component of interest in the vector defined by Eq. (14) is the transverse tip displacement.

The moduli of the power FRFs obtained from the FE model (thinner lines) for five different values of load resistance are plotted in Fig. 2a. These FRFs are in good agreement with the analytically obtained curves (Erturk and Inman, 2008b) (thicker lines). The mechanical vibration (motion transmissibility) FRFs of the unimorph obtained from the FE model and the analytical solution are presented in Fig. 2b.

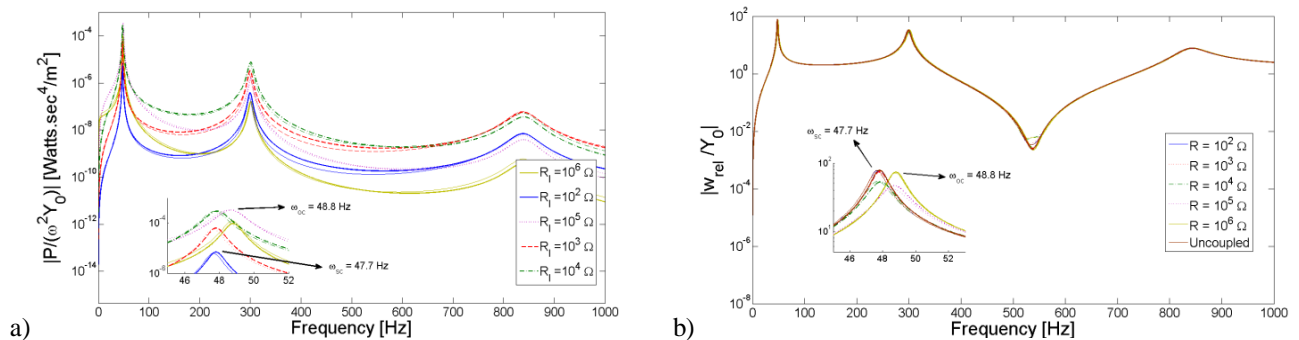


Figure 2. a) Power FRFs for five different values of load resistance with the enlarged view of mode 1. b) Relative tip motion FRFs for five different values of load resistance with the enlarged view of mode 1.

The voltage FRF has a monotonic behavior with increasing load resistance for every excitation frequency. That is, the voltage across the resistive load increases with increasing load resistance and the frequency of maximum voltage output moves from short circuit (ω_{sc}) to open circuit (ω_{oc}) resonance frequency. The electrical current FRF exhibits an opposite behavior (Erturk and Inman, 2008b, De Marqui et al., 2009). The product of voltage and current FRFs gives the electrical power FRF, which shows intersections between the curves of different electrical resistances (Fig. 2a). That is, at a fixed frequency, the variation of peak power output with load resistance is not monotonic (enlarged view of the first mode plotted in Fig. 2a). Although the difference between the short circuit resonance frequency (47.8 Hz) and the open circuit resonance frequency (48.8 Hz) is just 1 Hz considerably different optimum load resistance values are obtained for them (Erturk and Inman, 2008b). The short circuit and the open circuit resonance frequencies predicted by the FE model are 47.7 Hz and 48.8 Hz respectively.

The mechanical vibration FRFs obtained from the FE model and the analytical solution are presented in Fig. 2b. As can be observed from the enlarged view of Fig. 2b, the vibration amplitude at short circuit resonance frequency (47.8 Hz) decreases as the load resistance is increased from $10^2 \Omega$ to $10^5 \Omega$. This is the resistive shunt damping effect associated with power generation. The motion at the open circuit resonance frequency (48.8 Hz) is amplified with increasing load resistance ($10^6 \Omega$). Simultaneous investigation of the enlarged views in Figs. 2a and 2b proves that the effect of piezoelectric coupling results in variation of natural frequencies and variation of the amplitudes of electrical

and mechanical outputs. The uncoupled FRF presented in Fig. 2b is the typical mechanical FRF (transmissibility) when no electromechanical coupling is considered. The electromechanically coupled vibration FRF converges to the uncoupled FRF when the value of load resistance tends to zero (short circuit conditions). The inaccuracy in the FE predictions around the anti-resonance in Fig. 2b is related to the FE mesh.

5.2. Case study 2 - Bimorph harvester with tip mass under base excitation

In the second case study, the results obtained from the electromechanical FE model are compared with the single-mode analytical predictions of the closed-form solution and experimental results presented by Erturk and Inman (2009) for a cantilevered bimorph with a tip mass under base excitation (Fig. 3). The bimorph harvester configuration has a brass substructure bracketed by two PZT-5A layers combined in series to the electrical load. Therefore the piezoceramic layers are poled in the opposite directions. Otherwise the electrical outputs would be cancelled.

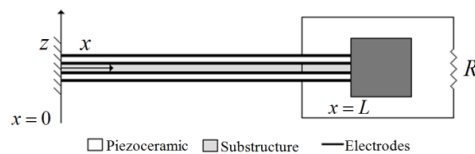


Figure 3. Bimorph piezoelectric energy harvester with a tip mass (series connection case).

For this case study the voltage FRF is defined as the voltage output per base acceleration (in terms of the gravitational acceleration, $g = 9.81\text{m/s}^2$) to be in agreement with the experimental and analytical voltage FRFs given by Erturk and Inman (2009). Equation (13) is easily modified to give voltage output per base acceleration. However the contribution of the additional piezoceramic layer and the contribution of the tip mass have to be added to the mass matrix as well as to the mechanical forcing term, since it is a function of the inertia of the structure in the base excitation problem. The contribution of the additional piezoceramic layer also affects the stiffness. The damping matrix is also modified since it is assumed proportional to the mass and stiffness matrices. The mechanical FRF is defined here as the velocity FRF (the ratio of the amplitude of velocity at the tip of the beam (relative to the fixed frame) to the gravitational acceleration) as it is measured by a laser vibrometer located on the fixed ground. This FRF is easily obtained from the expression of the relative tip motion FRF (Eq. (14)) using $-jg / \omega(1 + \mathbf{w}_{rel}(L, t) / Y_0)$. Here the effective piezoelectric coupling term in the series connection case is equal to the contribution of one piezoceramic layer and the effective capacitance is equal to one half of the contribution of one piezoceramic layer. The parameters used in the simulations are presented in Tables 1 and 3.

Table 3. Geometric and material properties of the bimorph harvester with tip mass

Length of the beam (m)	0.0508	Mass density of the substructure (kg/m^3)	9000
Width of the beam (m)	0.0318	Thickness of the PZT (each) (m)	0.0026
Thickness of the substructure (m)	0.0014	Proportional constant $-\alpha$ (rad/s)	14.65
Young's modulus of the substructure (GPa)	105.0	Proportional constant $-\beta$ (s/rad)	10^{-5}
Tip mass (Kg)	0.012		

The voltage FRFs for the first mode of the bimorph harvester with tip mass obtained from the FE model are plotted in Fig. 4a along with the analytical solution and experimental results for eight different values of load resistances (1, 6.7, 11.8, 22, 33, 47, 100, 470 $\text{k}\Omega$). The monotonic behavior of voltage output with increasing load resistance is observed for all excitation frequencies according to the numerical (FE model), analytical and experimental results. The experimental short circuit and open circuit resonance frequencies for the harvester are 45.6 Hz and 48.4 Hz, respectively. The analytical model predicts these frequencies as 45.7 Hz and 48.2 Hz, respectively. The FE model predictions of the short circuit and open circuit resonance frequencies are 45.7 Hz and 48.3 Hz, respectively.

It is observed in Fig. 4b that the mechanical FRFs obtained from the FE model are in agreement with the analytical and experimental results. The vibration amplitude at the short circuit resonance frequency is attenuated as the load resistance is increased up to 100 $\text{k}\Omega$. Approximately after this value of load resistance, increasing load resistance amplifies the vibration amplitude at the open circuit resonance frequency and the vibration amplitude at the short circuit resonance frequency is no longer attenuated.

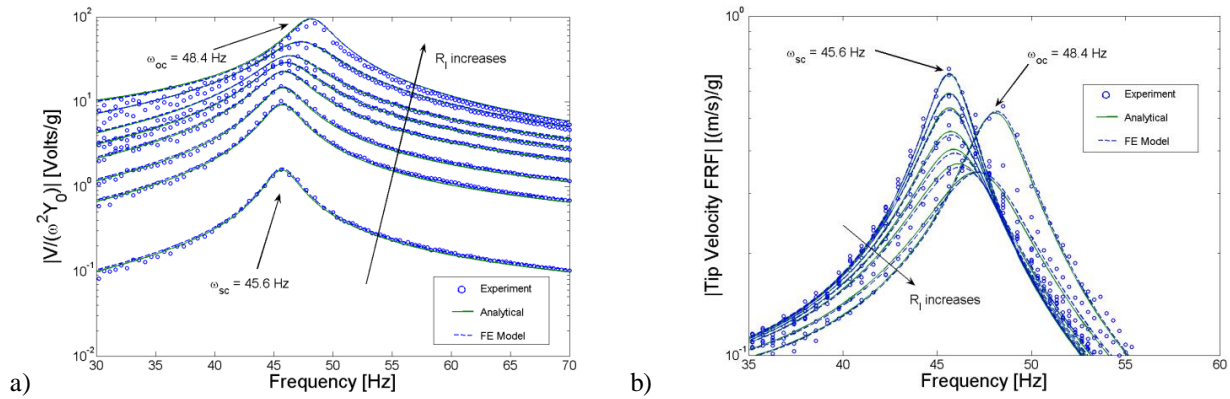


Figure 4. a) Voltage FRFs for eight different values of load resistance. b) Velocity FRFs for eight different values of load resistance.

5.3. Case study 3 – Piezo-aero-elastic behavior of a generator wing

This section presents the piezo-aero-elastic behavior of a cantilevered plate-like wing with embedded piezoceramics as the third case study. Two identical layers of PZT-5A are embedded into the top and on the bottom of the plate. Conductive electrodes bracketing the piezoceramic layers (poled in the opposite directions) are connected in series to a resistive electrical load as depicted in Fig. 5.

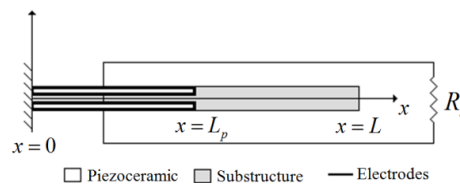


Figure 5. Generator wing with embedded piezoceramics (series connection).

The dimensions of the plate-like wing used in this work are $1200 \times 240 \times 3 \text{ mm}^3$. The identical embedded piezoceramic layers have the same width as the wing chord. The embedded piezoceramics layers cover 30% of the wing span (from the root to the tip) and each one has a thickness of 0.5 mm. The geometric and material properties of the plate-like wing (aircraft aluminum alloy Al 2024-T3) are presented in Table 4. The material and electromechanical properties for PZT-5A are given in Table 1.

Table 4. Geometric and material properties of the aluminum wing.

Length of the wing (mm)	1200	Mass density (kg/m^3)	2750
Width of the wing (mm)	240	Proportional constant $-\alpha$ (rad/s)	0.1635
Thickness of the wing (mm)	3	Proportional constant $-\beta$ (s/rad)	4.1711×10^{-4}
Young's modulus (GPa)	70.0		

The mode sequence and the undamped natural frequencies for the plate-like wing obtained from the FE model for short-circuit conditions (very low load resistance) is 1st B (1.68 Hz), 2nd B (10.46 Hz), 1st T (16.66 Hz), 3rd B (27.74 Hz) and 2nd T (48.65 Hz). Here B and T stand for the bending modes and torsion modes, respectively. The span-wise elastic axis and the center of gravity are coincident at 50% of chord.

One can observe in figures 6a and 6b the piezo-aero-elastic behavior of the generator wing for the short-circuit conditions. Figure 6a shows the frequency content of the five modes considered during the simulation. For the airflow speeds smaller than 20 m/s the frequencies are still similar to the undamped natural frequencies (which is given for the case without airflow). Increasing airflow speed results in coupling among the modes. For the airflow speed of 40 m/s the modes are coupled at the flutter frequency (12.2 Hz) and the motion of the plate-like generator wing is quite dominated by a second bending mode with some torsion coupling. The variation of total damping ratio (summation of structural damping and aerodynamic damping) for the second vibration mode (2nd B, 10.46 Hz) with increasing airflow speed is presented in figure 6b. Damping has a major effect in vibration-based power harvesting. Therefore larger mechanical amplitudes and consequently larger power outputs are expected for large aerodynamic loads and low damping which is the case for airflow speeds around the flutter condition.

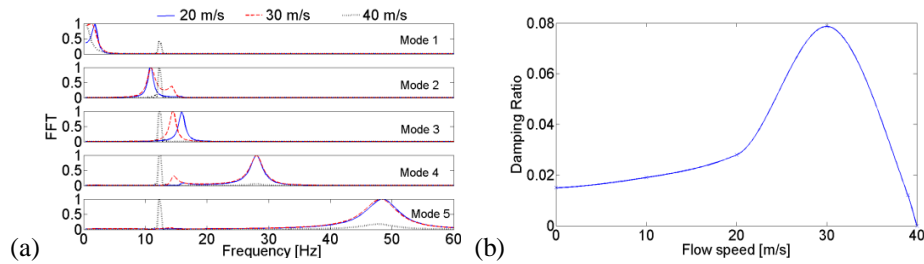


Figure 6. (a) Frequency content for three different flow speeds; (b) variation of total (structural and aerodynamic) damping ratio with increasing flow speed.

The time history of power output for the flutter speed is shown in figure 7a. The power output increases as the value of load resistance is increased from $R_l = 10^2 \Omega$ to $R_l = 10^4 \Omega$ as can be observed in figure 7a. Power output is continuously extracted over the time in this underdamped case. Clearly the value of load resistance $R_l = 10^4 \Omega$ provides the maximum power output among the set of load resistances considered here. Note that the time history with the largest power for this load resistance shows a decaying behavior which is due to the strong shunt damping effect of power generation, what can also be verified in figure 7b. If R_l is increased to $10^5 \Omega$, the amplitude of power output decreases. When the load resistance is further increased to $10^6 \Omega$ (open circuit condition) the power output is considerably reduced to values similar to the values obtained for $R_l = 10^2 \Omega$ (enlarged view in figure 7a).

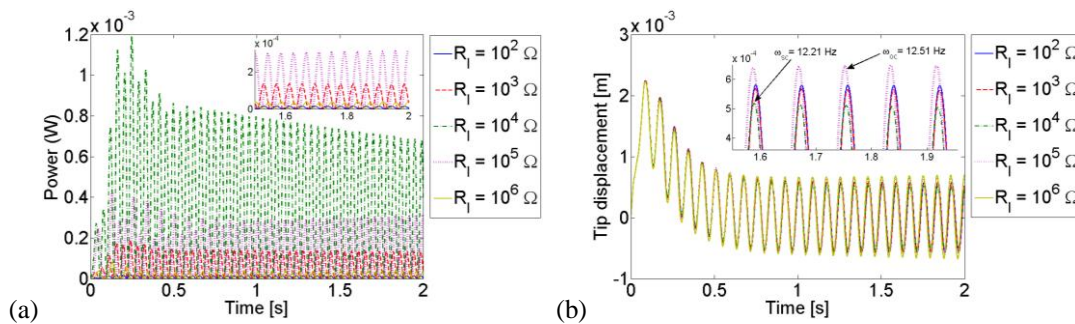


Figure 7. (a) Power output and (b) tip displacement for five different values of load resistance at the flutter speed.

6. CONCLUSIONS

In this paper, an electromechanical FE based on the classical plate theory is derived for piezoelectric energy harvesting from base excitations. The electromechanical FE model is derived based on generalized Hamilton's principle for electroelastic bodies and it accounts for the presence of a pair of conductive electrodes covering the entire piezoceramic layer. A resistive electrical load is considered in the electrical domain. Derivations are given for predicting the coupled mechanical vibration and electrical power response of the harvester plate due to base excitation. The electromechanical FRFs obtained from FE model are in very good agreement with the analytical results obtained from the closed-form solution for a unimorph cantilever under base excitation. The electromechanical FE model can also predict the analytical and the experimental results of the bimorph cantilever with a tip mass reported in the literature. In both cases the electromechanical behavior is investigated for several values of external load resistances.

A piezo-aero-elastic analysis of a plate-like wing with embedded piezoceramics is also presented. The piezo-aero-elastic model is obtained by combining an electromechanically coupled FE model and an UVLM. The conversion of aeroelastic vibrations into electrical energy is investigated at several airflow speeds for a set of electrical load resistance. The piezo-aero-elastic behavior at the flutter speed is presented in detail. The maximum aerodynamic damping is observed for airflow speeds around 30 m/s. Therefore this is not a favorable condition for persistent electrical response as the motion decays rapidly. The most favorable conditions for power harvesting occur for airflow speeds higher than 30 m/s and especially for very low values of aerodynamic damping. At the flutter speed, the aerodynamic damping vanishes and the oscillations are persistent. Although this condition is avoided in a real aircraft, this is the best condition as a concept demonstration for the generator wing.

In addition to the benefit of electrical power generation from aeroelastic vibrations, the resistive shunt damping effect is observed. It is possible to determine an optimum value of load resistance for each airflow speed and the amplitude of motion is reduced especially for the loads yielding the largest power output. When the value of load resistance is further increased (larger than optimum value) the amplitude of motion increases and the system oscillates at open circuit frequency of a given airflow speed. A critical situation is observed at the flutter speed. Close to the open

circuit conditions (for $10^5 \Omega$ and $10^6 \Omega$) the neutral stability observed at the flutter speed for short circuit condition is converted to an unstable motion. For the optimum value of load resistance ($10^4 \Omega$) the neutral stability of the wing at the flutter speed for short circuit conditions is converted to a stable response.

7. ACKNOWLEDGEMENTS

The authors gratefully acknowledge the support of the Air Force Office of Scientific Research MURI under grant number F 9550-06-1-0326 “Energy Harvesting and Storage Systems for Future Air Force Vehicles” monitored by Dr. B. L. Lee. The authors also gratefully acknowledge the support of CAPES (Brazil).

8. REFERENCES

- Anton, S. R. and Sodano, H. A., 2007, “A Review of Power Harvesting Using Piezoelectric Materials (2003–2006),” *Smart Mater. Struct.*, Vol. 16, pp. R1–R21.
- Anton, S. R., and Inman, D. J., 2008, “Vibration Energy Harvesting for Unmanned Air Vehicles,” *Smart Structures and Materials 2008: Active and Passive Smart Structures and Integrated Systems II*, March 10-13, San Diego, CA. Proc. SPIE Vol. 6928.
- Beeby, S. P., Tudor, M. J. and White, N. M., 2006, “Energy Harvesting Vibration Sources for Microsystems Applications, *Measurement Science and Technology*, Vol. 13, pp. 175-195.
- Benini, G.R., Belo, E.M. and Marques, F.D., 2004, “Numerical Model for the Simulation of Fixed Wings Aeroelastic Response”, *Journal of the Brazilian Society of Mechanical Sciences & Engineering*, Vol. 26, pp. 129-136.
- Chen, S.-N., Wang, G.-J., and Chien, M.-C., 2006, “Analytical Modeling of Piezoelectric Vibration-Induced Micro Power Generator,” *Mechatronics*, Vol. 16, pp. 397–387.
- Cook-Chennault, K. A., Thambi, N. and Sastry, A. M., 2008, “Powering MEMS portable devices – a review of non-regenerative and regenerative power supply systems with emphasis on piezoelectric energy harvesting systems”, *Smart Materials and Structures*, Vol. 17, 043001.
- De Marqui, Jr., C., Erturk, A., and Inman, D.J., 2009, “An Electromechanical Finite Element Model for Piezoelectric Energy Harvester Plates”, *Journal of Sound and Vibration (in press)*.
- Dodemant L. R., 2007, Multifunctional structures for spacecraft: Embedded lithium-ion batteries, MSc Thesis Cranfield University.
- duToit, N. E., Wardle, B. L., and Kim, S., 2005, “Design Considerations for MEMS-Scale Piezoelectric Mechanical Vibration Energy Harvesters,” *Integr. Ferroelectr.*, Vol. 71, pp. 121–160.
- Erturk, A. and Inman, D. J., 2009a, “An experimentally validated bimorph cantilever model for piezoelectric energy harvesting from base excitations,” *Smart Materials and Structures*, 18 025009
- Erturk, A. and Inman, D.J., 2008b, “A Distributed Parameter Electromechanical Model for Cantilevered Piezoelectric Energy Harvesters,” *ASME Journal of Vibration and Acoustics*, Vol. 130, 041002.
- Erturk, A., Renno, J. R. and Inman, D. J., 2008a, “Modeling of Piezoelectric Energy Harvesting from an L-shaped Beam-Mass Structure with an Application to UAVs, *Journal of Intelligent Material Systems and Structures*, Vol. 20, pp. 529-544.
- Lambert, J.D., 1991, “Numerical Methods for Ordinary Differential Systems: The Initial Value Problem”, Chichester: Wiley.
- Lin, J.H.; Wu, X.M.; Ren, T.L. and Liu, L.T., 2007, “Modeling and simulation of piezoelectric MEMS energy harvesting device”, *Integrated Ferroelectrics* Vol. 95, pp. 128-141.
- Magoteaux, K. C., Sanders, B., and Sodano, H. A., 2008, “Investigation of energy harvesting small unmanned air vehicle,” *Smart Structures and Materials 2008: Active and Passive Smart Structures and Integrated Systems II*, March 10-13, San Diego, CA. Proc. SPIE Vol. 6928.
- Pines, D.J. and Bohorquez, F., 2006, “Challenges Facing Future Micro-Air-Vehicle Development”, *Journal of Aircraft*, Vol 43, pp. 290-305.
- Priya, S., 2007, “Advances in energy harvesting using low profile piezoelectric transducers” *Journal of Electroceramics* Vol. 19, 167–184.
- Roundy, S., Wright, P. K. and Rabaey, J., 2002, “Micro-electrostatic vibration-to-electricity converters”, *Proceedings of the ASME 2002 International Mechanical Engineering Congress and Exposition*.
- Roundy, S., Wright, P. K., and Rabaey, J. M., 2003, “A Study of Low Level Vibrations as a Power Source for Wireless Sensor Nodes,” *Comput. Commun.*, Vol. 26, pp. 1131–1144.
- Sodano, H. A., Park, G., and Inman, D. J., 2004, “Estimation of Electric Charge Output for Piezoelectric Energy Harvesting,” *Strain*, Vol. 40, pp. 49–58.

9. RESPONSIBILITY NOTICE

The authors are the only responsible for the printed material included in this paper.